

A cryostatic, fast scanning, wideband NQR spectrometer for the VHF range

Hermann Scharfetter, Markus Bödenler, Dominik Narnhofer

Institute of Medical Engineering, Stremayrgasse 16, Graz University of Technology, 8010
Graz

Corresponding Author: Hermann Scharfetter, hermann.scharfetter@tugraz.at

Published article: H. Scharfetter, M. Bödenler, and D. Narnhofer, 'A cryostatic, fast scanning, wideband NQR spectrometer for the VHF range', *J. Magn. Reson.*, vol. 286, pp. 148–157, Jan. 2018. <https://doi.org/10.1016/j.jmr.2017.12.004>

This manuscript version is made available under the CC-BY-NC-ND 4.0 license
<http://creativecommons.org/licenses/by-nc-nd/4.0/>

Abstract

In the search for a novel MRI contrast agent which relies on T_1 shortening due to quadrupolar interaction between Bi nuclei and protons, a fast scanning wideband system for zero-field nuclear quadrupole resonance (NQR) spectroscopy is required. Established NQR probeheads with motor-driven tune/match stages are usually bulky and slow, which can be prohibitive if it comes to Bi compounds with low SNR (excessive averaging) and long quadrupolar T_1 times. Moreover many experiments yield better results at low temperatures such as 77K (liquid nitrogen, LN) thus requiring easy to use cryo-probeheads. In this paper we present electronically tuned wideband probeheads for bands in the frequency range 20 – 120 MHz which can be immersed in LN and which enable very fast explorative scans over the whole range. To this end we apply an interleaved subspectrum sampling strategy (ISS) which relies on the electronic tuning capability. The superiority of the new concept is demonstrated with an experimental scan of triphenylbismuth from 24 – 116 MHz, both at room temperature and in LN. Especially for the first transition which exhibits extremely long T_1 times (64ms) and low signal the new approach allows an acceleration factor by more than 100 when compared to classical methods.

Keywords: nuclear quadrupole resonance, bismuth compounds, wideband cryo-probehead, varactor diodes, tuning and matching, interleaved subspectrum sampling

Highlights

- Fast electronically tuneable wideband cryo-coils for NMR and NQR spectroscopy
- electronic tuning/matching allows for very short repetition times
- fast interleaved subspectrum sampling for very short repetition times even at long T_1
- strong acceleration of explorative wideband NQR scans by factors of 100 and more

1. Introduction

During the last decades significant efforts have been made to establish magnetic resonance imaging (MRI) in the context of cellular and molecular imaging so as to provide spatially and temporally resolved maps of biomarkers which contain information on pathophysiological processes correlated with cancer and other diseases [1]. So far, however, the relatively low sensitivity requires special signal enhancement strategies, mostly by the administration of an extrinsic tracer or contrast agent (CA) [2] which shorten either predominantly T_1 (e.g. gadolinium based paramagnetic chelates) or T_2 (e.g. paramagnetic iron oxide nanoparticles) relaxation time of free water protons [3]. In the last years many concepts have been elaborated for “smart” contrast agents that exhibit a change in relaxivity upon activation. Image contrast can be switched in response to physiological alterations such as pH, temperature, metal ions, redox state and enzyme activity [4] [5].

Lately, chemical exchange saturation transfer (CEST) has gained interest as an alternative MRI contrast mechanism. CEST contrast can be switched on and off using a selective radio frequency (RF) saturation pulse but suffers from low sensitivity, specific absorption rate (SAR) restrictions and saturation spill-over effects between bulk protons and protons of the CEST agent due to insufficient frequency separation [6],[7]. Recently new metal-free T_2 shortening agents have been reported which rely on nitroxide-based macromolecules [8] and which have the advantage of being free of toxic heavy metals. However, as they represent radicals, their lifetime may become limiting and they are not inherently switchable.

An interesting alternative to the established approaches could be the exploitation of so-called quadrupolar relaxation enhancement (QRE), which means the shortening of T_1 by the interaction of protons with quadrupolar nuclei (QN), i. e. nuclei with a spin quantum number ≥ 1 which possess an electric quadrupolar moment. The effectiveness of QRE for producing MRI contrasts has been proven for the interaction between ^1H and ^{14}N in the amide groups of proteins at very low magnetic fields [9],[10],[11],[12] but is completely unexplored in the context of extrinsic CAs at clinical fields such as 1.5 or 3T.

QRE, in contrast to most other mechanisms for relaxation enhancement, is frequency selective, because it can only become effective if the proton Larmor frequency comes close to one of the transition frequencies of the QN [12]. This feature opens the possibility to switch on and off QRE by changing the static magnetic flux density B_0 . As the latter depend

on the electronic environment of the QN, QRE is also sensitive to changes of e.g. the chemical bonding structure, which opens many opportunities for chemically selective contrasts.

For several reasons (high spin quantum number 9/2, high natural abundance, rich chemistry, suitable quadrupolar coupling constant Q_{cc}) ^{209}Bi appears as an especially attractive QN. It is considered as comparatively non-toxic and thus compounds are expected to have a higher biocompatibility than e. g. gadolinium based CAs. ^{209}Bi is being suggested [13] [14] also in x-ray contrast agents which makes it an ideal candidate for dual-mode CAs for CT and MRI with only a single core element. ^{209}Bi is particularly interesting because there exist several inorganic and organometallic compounds with transition frequencies already close to those required at clinical field strengths, e.g. 3T.

The development of Bi-based contrast agents employing QRE at defined frequencies involves several steps, the detailed discussion of which exceeds the scope of this paper. In any case, however, the transition frequencies of the synthesized compounds must be determined, which, in most cases, can be done easiest with zero-field nuclear quadrupole resonance spectroscopy (NQRS). NQRS has several applications in solid state physics e.g. for the investigation of chemical bonds and crystal structures [15][16], the real-time detection of specific toxic species (e.g. arsenic) in minerals [17] or the detection of explosives [18] and drugs [19] and the characterisation of pharmaceutical products [20]. Most current applications refer to ^{14}N with very low relevant frequencies up to only several MHz. In contrast, the characterization of suitable Bi compounds requires NQRS in the VHF range, because the ^1H Larmor frequencies of most clinical MRI systems range from several tens of MHz (e.g. 64 MHz@1.5T) up to 130MHz (3T) or even 300 MHz (7T). The identification of still unknown peaks in newly synthesized ^{209}Bi compounds and their full spectral characterization requires the scanning over many tens of MHz due to the presence of at least four transition frequencies in spin-9/2 nuclei. Thus the typical resonators in NMR probeheads cannot be used because of their small bandwidth. In order to circumvent this problem, commercially available probeheads are equipped with stepper motor drives which mechanically control the tuning and matching capacitors. Though robust and low-loss such implementations have their disadvantages, i. e. they are comparatively large, heavy and slow. As will be shown, in the case of samples with low SNR and long T_1 times such an approach renders NQRS extremely tedious due to the need for excessive averaging with long repetition times. This problem can become stringent when measuring at low temperatures, e.g. in liquid nitrogen (77K), which is sometimes necessary in order to increase the SNR by population enhancement and, in favourable cases, a decrease of the transversal relaxation rate.

The aim of this paper is to present a very efficient solution which allows for a fast wideband scanning strategy based on a previously developed hybrid probehead which combines wideband transmit (TX) with electronically tuned and matched narrowband receive (RX) [21]. First we describe the modification of the hardware for operation at temperatures down to 77K (liquid nitrogen) and second we introduce an interleaved subspectrum sampling (ISS) sequence which relies on the rapid electronic tuning capability. Finally experiments with two promising ^{209}Bi -containing core-compounds for QRE will show the usefulness of the presented methodology.

2. Methods

Fast scanning strategy

In NMR spectroscopy bands of several 100 kHz can be excited by an appropriately controlled RF pulse sequence like e.g. the double-frequency sweep method [22] or related concepts [23] [24] and the WURST-QCPMG sequence [25]. However, as described in the excellent review about wideline acquisition by R. Schurko in [26], bandwidths of more than a few 100kHz require a frequency stepping method, which is especially true for explorative NQRS scans over tens of MHz. One of the limiting factors for the overall duration of an experiment is the repetition time T_R , which in the case of FID or spin echo sequences is typically greater than the longitudinal relaxation time T_1 . To increase the SNR mostly N spectra have to be averaged, and therefore the overall acquisition time per frequency is $N \cdot T_R$. Samples with long T_1 thus require long acquisition times.

Frequency stepping basically consists in repeating the above procedure for M different center frequencies into which the whole frequency span FS is subdivided [27], [28]. The resolution $\Delta f = FS/M$ is a function of the sampling rate, the acquisition window length and the minimum expected peak width. Basically there are 2 different possibilities for the frequency stepping strategy: (1) At every pulse frequency N datasets are acquired and averaged before hopping to the next frequency (2) Complete wideband spectra are acquired by sweeping N times through the M frequencies and doing the averaging afterwards. Strategy (1) is common with commercial NMR consoles while strategy (2) is the way many network analyzers (NWA) do their job.

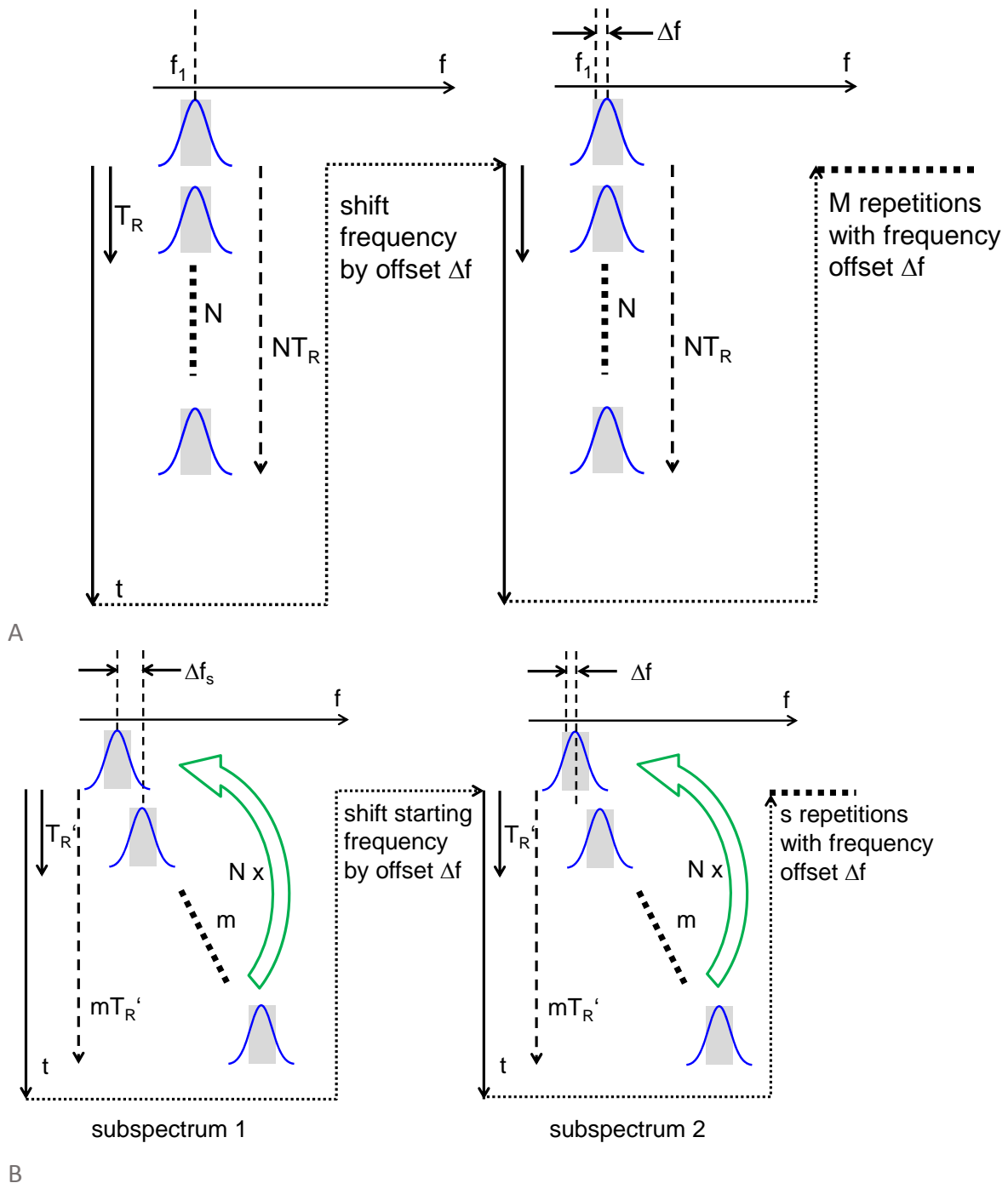


Fig. 1. A: Classical sampling strategy: N data points are averaged per loop, M loops with frequency offset Δf are accomplished. $T_R \geq T_1$

B: Fast interleaved subspectrum sampling: s coarsely spaced, interleaved subspectra are subsequently acquired in $s=M/m$ loops with frequency offset Δf . Within each loop averaging over N repetitions is accomplished (symbolized by the green curved arrows). $T_R' \geq T_1/m$

At a first glance the two strategies may appear equivalent. However, with strategy (2) the whole procedure can be accelerated significantly by interleaved subspectrum sampling (ISS), as illustrated in fig.1. Panel A shows the classical strategy, where N data points are acquired per acquisition loop and a simple spin echo sequence is assumed. Then the frequency is

shifted by Δf and the procedure is repeated M times, giving a total measurement time of $T_R * M * N$, where $T_R \geq T_1$.

Fig.1B illustrated the ISS, where FS is subdivided into $m \leq M$ frequency points the separation Δf_s of which corresponds at least to the bandwidth BW_{TX} of the TX pulse. In this case we have $\Delta f_s = FS/BW_{TX}$ and consequently $m = M * \Delta f / \Delta f_s$. In one acquisition loop N sub-spectra are acquired by sweeping through the m frequency points before averaging them. As each TX pulse only excites spin populations within its bandwidth, populations at the neighboring TX frequencies cannot be saturated and thus the available recovery time for each population is $m * T_R'$ instead of T_R . The requirement $T_R \geq T_1$ can be relaxed to $T_R' \geq T_1/m$, thus allowing for the much shorter repetition times $T_R' = T_R/m$.

In total a number $s = M/m$ of such loops must be accomplished in order to re-compose the original spectrum from the coarsely spaced sub-spectra whereby in each loop i the respective starting frequency must be shifted with respect to the previous loop $i-1$ by the wanted resolution Δf (see fig. 1B, subspectrum 2). In this way the total number of frequency points acquired is again M with a resolution of Δf .

However, the total measurement time T_{meas} after assembling and averaging of all subspectra is then $T_{meas} = T_R' * m * N * s = T_R' * M * N$ which is by a factor of m less than for the classical case. Because the number of required datasets is the same for both methods, the maximum acceleration factor is m .

For a better illustration assume a sample with $T_1 = 10$ ms with a weak signal which requires $N=1000$ averages. The explorative scan should cover $FS=12$ MHz and the resolution is set to $\Delta f = 20$ kHz, thus yielding $M=600$ frequency points. A spin echo sequence with rectangular pulses $T_P(90^\circ)=10\mu s$, $T_E=100\mu s$, $T_{DAQ}=50\mu s$ is applied. The bandwidth of such a pulse for more than 50% effectivity (FWHM) in the small flip angle limit is $1.21/T_P$ [29] i. e. roughly 120kHz. For simplicity let T_R be equal to T_1 , which yields $T_{meas}=1000 \times 600 \times 10$ ms = 6000s = 100 min for the classical scan.

Acquisition with ISS requires $m = 12\text{MHz}/120\text{kHz} = 100$ frequency points per subspectrum and $s=6$ subspectra for splitting Δf_s into 20 kHz steps. Thus T_R' can be chosen as short as $T_1/m=100\mu s$, which reduces T_{meas} to 1 min, i. e. one hundredths of the time needed for the classical technique.

The classical technique works fairly well with the slow tuning/matching elements driven by stepper motors, because the averaging of N datasets is accomplished before every re-tune/re-match step. If the averaging lasts much longer than the re-tuning procedure, there is not much delay. ISS, in contrast, requires re-tuning after every T_R' and is thus only possible with fast electronically tuned probeheads. Thus the tuning/matching elements must settle within T_R' , i. e. in less than $100\mu s$ for the shown example. This is clearly impossible with motor drives but very well feasible with varactors. There are, however, two limitations for the acceleration factor: (1) For a spin echo sequence T_R' cannot be shorter than $T_P/2 + T_E + T_{DAQ}/2$, whereby T_E is the echo time and T_{DAQ} the window length for data acquisition. (2) Shorter T_R' increases the duty cycle of the RF pulses and thus the average

power dissipation in the probehead. Therefore in practice the shortest T_R' used in our probeheads was 500 μ s.

Probehead circuitry

The probehead electronics is an advanced version of the one in [21] where the basic concept has been described in detail. Thus only the essential ideas shall be recapitulated very briefly. As shown in fig. 2 the circuit is subdivided into the passive TX network and the electronically tuned and matched RX circuitry.

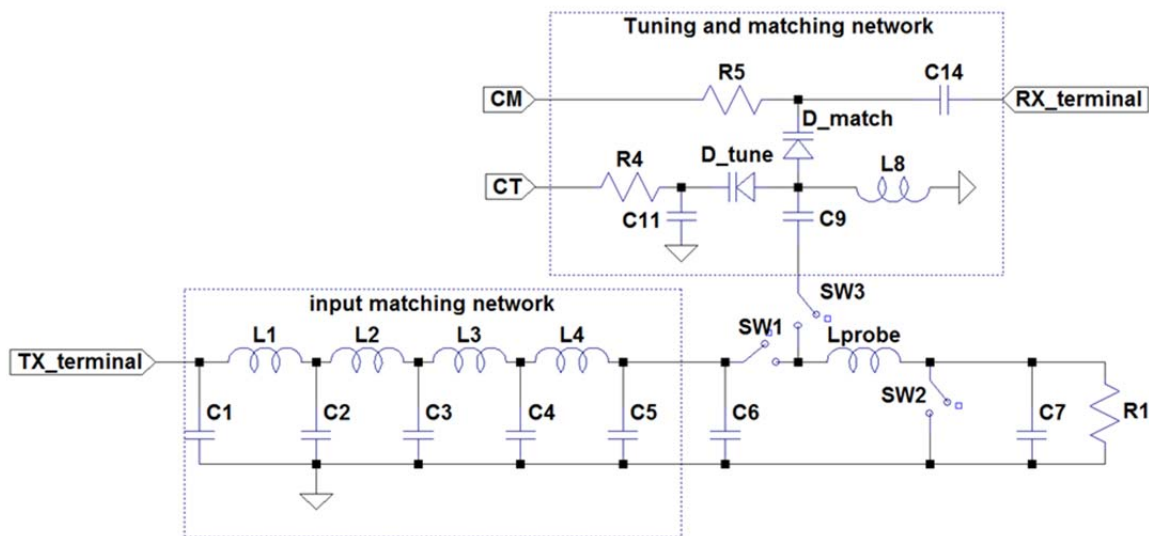


Fig. 2. Principle of the TX/RX matching circuitry (from [21]). During TX switch SW_1 is closed while SW_2 and SW_3 are open. During RX all switch states are reversed. The numbering of the components is not strictly monotonic because some parts have been left out for the sake of simplicity. It is, however, consistent with the detailed schematic in fig. 4.

During TX switch SW_1 is closed while SW_2 and SW_3 are open and hence power is passed to the termination resistor R_1 via a reactive network which represents a lumped exponential transmission line (LETL). It consists of the input matching network and the pi-section C_6, C_7 and L_{probe} and transforms the termination resistance R_1 into the 50 Ω input impedance over a large bandwidth, thus providing maximum current in the probe coil L_{probe} . During this phase the tuning/matching network is isolated from the circuitry by the open SW_3 . During RX L_{probe} is isolated from the power path by opening SW_1 and connected to the tuning/matching section by closing SW_2 and SW_3 . The NMR signal can now be received in resonator mode with high quality factor Q and passed to the 50 Ω port 'RX_terminal'. Tuning and matching is achieved with the varactors D_{tune} and D_{match} which are controlled via the reverse bias voltages provided at the ports CT and CM and which can settle fast enough for ISS.

For cryo-applications we have modified the previous probeheads according to the cross sectional drawing in fig 3. It consists roughly of a printed circuit board (PCB) with the RF

electronics and connectors as well as the probe coil assembly. The latter is supported by a hollow PTFE tube which carries at its tip the probe coil and along its outer surface a stripline which connects the coil with the PCB. A thin outer plastic tube protects the assembly and serves as a guide for cooling gas as well as a certain thermal insulation between the grounding copper of the stripline and the coolant. The probe coil can be either immersed directly into liquid nitrogen (LN) or inserted into a cryostat. The cold vapor of the LN or any other cooling gas can escape through the inner bore of the PTFE tube and removed at the nozzle protruding from the top side of the PCB. A thermal insulator made from polystyrene foam protects the PCB from excessive cooling and both the bottom of the PCB as well as the nozzle carry electric heaters so as to prevent the condensation of water along cold parts which are exposed to air humidity.

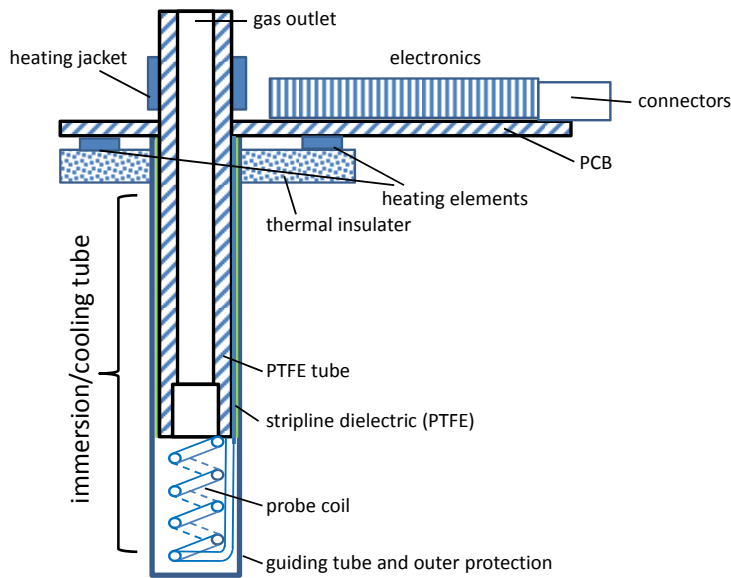


Fig. 3. Lateral cross-section of the probehead,

The choice of the values of all the inductances and capacitances of the LETL must obey a strict rule which follows from defining the center frequency f_c , the transform ratio $R_1/50\Omega$ and the number of pi-sections. The TX bandwidth BW_{TX} is then typically between 40 and 50% of f_c , depending on the definition of the useful bandwidth. In our case we define BW_{TX} as the one within which the magnitude of the input reflexion factor S_{11} at the TX terminal does not exceed -10dB, a value which is tolerated by most RF power amplifiers. The choice of R_1 determines the Q-factor of the probe coil, because, as detailed in [21], the inductance of the latter is proportional to R_1 . With a number of pi-sections ≥ 4 and R_1 ranging between 10Ω and 200Ω the relationship between L_{probe} and R_1 is approximately

$$L_{probe} \approx \frac{R_1}{2\pi f_c} \quad (1)$$

and

$$Q \approx \frac{f}{f_c} \frac{R_1}{r} \quad (2)$$

where f is the actual operating frequency and r is the loss resistance of the probe coil. In contrast to [21] R_1 was set to 100Ω , which implies comparatively high L_{probe} and Q as well as an up-transformation of the voltage by a factor of $\sqrt{\frac{R_1}{50\Omega}}$ i.e. 1.41. The current, in turn is transformed down by the same factor. Both effects have advantages and disadvantages. On one hand some elements, especially the capacitors C_6 and C_7 and the switches SW_2 and SW_3 must withstand comparatively high voltages (approx. $141 V_{\text{peak}}$ at an RF power of 100W), but on the other hand the resistive losses and the thermal stress of SW_1 decreases by a factor of 2.

The detailed schematic of the RF circuitry is shown in fig. 4. For comparison, all common components are numerated in the same way as in fig. 2. Component values have been omitted intentionally because they depend on the individual frequency bands. Instead design rules are being discussed.

As in [21] PIN diodes (MA4P7104F-1072T, MACOM) were used for SW_2 and SW_3 but SW_1 was replaced by the crossed diodes $D_1 - D_4$ with low reverse recovery time (BAS316, NXP). A quadruple was used instead of the pairs commonly described in textbooks in order to increase the allowed power dissipation. Crossed diodes are very common (cf. e.g. [30]) but their downside is the higher parasitic capacitance (here typ. 2.5 pF per quadruple) when compared to a reverse-biased PIN diode of similar power ratings (here 0.7 pF). Coupling between the TX matching network and the probe coil via these parasitic capacitances can significantly lower the Q -factor during RX, especially at high frequencies (70MHz and above). Thus for the highest frequency band each diode was replaced by a series of two or three diodes so as to reduce the total capacitance to less than 1 pF. The crossed switching diodes D_8 and D_7 protect the sensitive varactors and the preamplifier following the RX port from high residual RF signals during TX.

$C_8 - C_{14}$ serve as RF shortcuts in the respective frequency bands. Their values should be as high as possible, but all of them are limited by timing considerations. C_{11} , C_{12} , C_{13} together with resistors R_4 and R_5 provide the reverse biasing of the varactors and must be chosen such that the bias voltage settles to within 1% in less than the minimum wanted repetition time T_R' , e.g. a few 100 μs for ISS. R_5 must be significantly higher than the typical RX load impedance of 50 Ω , e. g. 1 k Ω while R_4 must be significantly higher than the reactance of C_{10} , typically several k Ω . Resistors were used instead of the usual inductive chokes because they do not produce spurious ringing after step changes of the bias voltages.

In the spectrometer the voltage at 'HV_PIN' is 250 V during all TX pulses (reverse bias) and -5V (forward bias) during the rest of the time. The resistors R_2 and R_3 in the biasing networks R_2/L_6 and $R_3/C_{10}/L_7$ limit the PIN diode forward bias currents to ca. 100mA and thus have 39 Ω , each. L_6 and L_7 serve as RF chokes while L_8 provides a common GND reference for D_6 and both varactors. The inductances must be chosen significantly higher than that of L_5 in order not to change the properties of the tank circuit. Moreover L_7 and L_8 must have high Q factors, because they lie in parallel to the probe coil from the RF viewpoint and their losses contribute directly to the resonator losses. These coils were thus fabricated with air core and

comparatively thick (0.4 mm) enamelled copper wire. In this context C_{10} plays an important role as RF shortcut so as to decouple the ohmic loss R_3 from L_7 .

C_8 and C_9 decouple the PIN diode bias paths from the RF path. They must be rated for ≥ 250 V and their capacitances must be kept as low as possible, providing still good RF passage but limiting the switching currents during the edges of the 250 V pulses to values which do not significantly afflict the rise time and the power demands for the control pulse source.

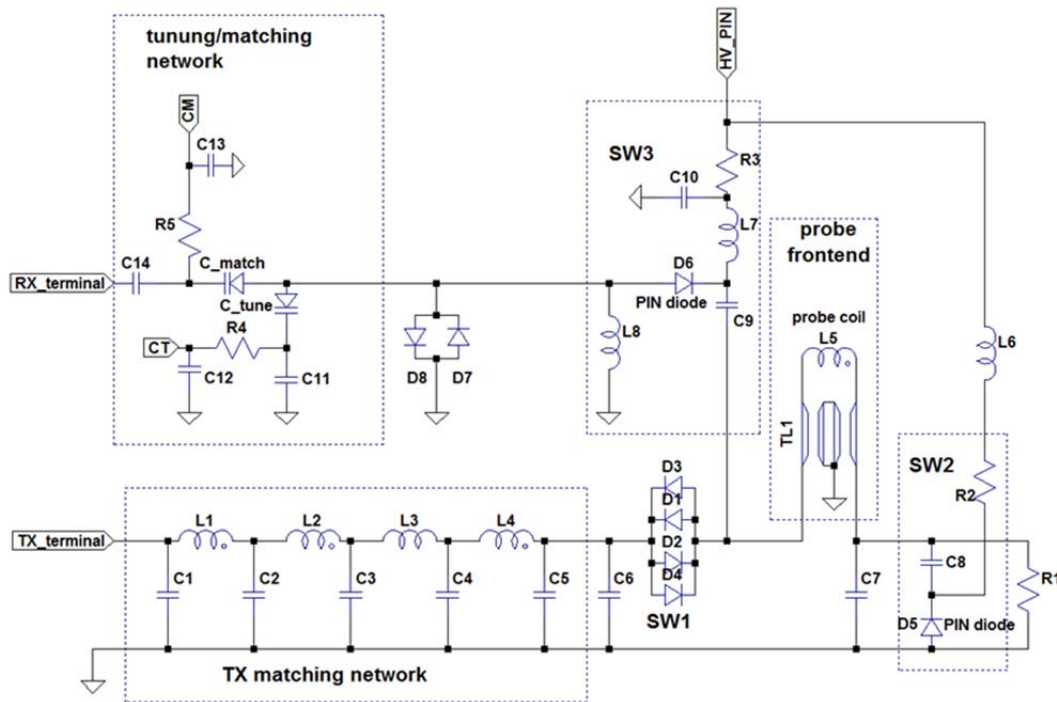


Fig. 4. Detailed schematic of the RF section of the PCB.

The design of the connection line TL_1 between the probe coil and the PCB deserves special attention because it requires a trade-off between partially conflicting goals:

(A) Thermal viewpoint:

(i) During cryo-applications a longer PTFE tube allows for deeper insertion into LN and/or for better thermal insulation between the PCB and the LN.

(ii) The connection line should have a small cross-section in order not to convey too much heat flux from the tip to the PCB, which increases consumption of coolant and the danger of condensation on the PCB

(B) RF viewpoint:

(iii) The connection line along the tube adds parasitic inductance in series with the useful part L_5 of the probe inductance, i.e. the one which actually receives the signal. As the total inductance is fixed according to eq 1 for a certain frequency band, the parasitic amount reduces the RX sensitivity and should be kept minimal. The parasitic inductance decreases with the area enclosed by the line conductors and typically increases with tube length.

(iv) The Q-factor is inversely proportional to the ohmic losses of L_{probe} . Therefore the cross-sectional circumference of the conductors of both L_5 and TL_1 should be large in order to account for the skin effect. Typically this also increases the cross-section of the respective conductors.

Requirements (i) and (iii) as well as (ii) and (iv) are contradictory, respectively, and thus a compromise must be found. A good solution is an edge-coupled symmetric microstrip line, because it allows for large surface/cross-section ratio of the conductors thus serving both (ii) and (iv). The gap between the strips should be small in order to satisfy (iii). The dielectric should be thin enough in order to prevent the current to concentrate close to the strip edges due to the proximity effect which would increase the losses. On the other hand the thickness must exceed a certain limit to prevent excessive capacitance per length which adversely affects the transformation properties of the line. In the simplest case (electrically short line) the even capacitances between strips and ground add to C_6 and C_7 , respectively, forcing their values to be reduced. The maximum allowable line length is reached when either of them is replaced entirely by the line capacitance which can be calculated from Z_0 and the phase velocity c :

$$Z_0 = \sqrt{\frac{L'}{C'}}; \quad c = \frac{1}{\sqrt{L' C'}} \quad (3)$$

$$C' = \frac{1}{c Z_0}, L' = \frac{Z_0}{c} \quad (4)$$

C' and L' denote the per-length capacitance and inductance, respectively. Therefore the maximum length can be approximated as

$$l_{\text{max}} = \frac{C_7}{C'} \quad (5)$$

Parametric simulations with LTSpice (Linear Technologies) were carried out to find out the best Z_0 at a certain desired length of the line so as to achieve maximum bandwidth both at TX and RX. Then the stripline geometry was calculated with a web-based stripline calculator (<https://www.eeweb.com/toolbox/edge-coupled-microstrip-impedance>) for the required Z_0 . The thickness of the dielectric was chosen with 0.5 mm for practical reasons. A PTFE sheet was chosen for the dielectric due to its low losses and low capacitance per length. As conductors we used self-adhesive copper foil with a thickness of 50 μm and a strip width of 3 mm. In order to minimize thermal contact with the coolant, the outermost copper part (in our case the GND layer) was insulated by a plastic tube which at the same time serves as a guide for the cooling gas around the probe coil (see fig. 3). As a general rule increasing the

frequency leads to shorter tubes because the capacitors must decrease inversely proportional to f_0 .

Let us give a practical example: Setting f_c to 95 MHz in order to get a useful TX band between 70 and 120 MHz requires a C_7 of ca. 17 pF. A reasonable value for Z_0 is 30Ω and c in a PTFE dielectric is approximately $2 \cdot 10^8$ m/s. Thus we obtain a L' of 150 nH/m and a C' of 167 pF/m. The maximum theoretical length of the tube is thus 9.7 cm. However, due to additional parasitic capacitances on the PCB, this value must be reduced so that in practice the typical length is 6-7 cm only. The effective parasitic inductance is then 17 nH which is less than 10% of L_5 and thus practically negligible. Going down in frequency to an f_c of say 30 MHz allows for a maximum tube length of >30 cm which is more than sufficient for most applications.

At high f_c a somewhat longer tube is possible at the cost of a reduced bandwidth with a modification of the circuit according to fig. 5. The difference to fig. 4 is the replacement of SW_3 by a passive RX protecting network consisting of two series connected lumped $\lambda/4$ line equivalents and two pairs of clamping diodes D_7/D_8 and D_{11}/D_{12} . This circuit is very common in NMR coils, see e.g. [30],[31]. The first $\lambda/4$ equivalent is formed by L_7 , C_9 and one half of C_{10} while the second one, less obviously, is built up by L_9 , the second half of C_{10} and a part of the tuning capacitance C_{tune} . The resonance frequency of this network is placed approximately in the center of the desired scanning bandwidth. Exactly at resonance the function of this circuit is obvious: During TX D_7/D_8 form the usual short-circuit which is transformed to an open end at the connection point with the probing coil and thus does not perturb the TX pulse. In turn the RX section is protected by the clamping diodes. The second pi-section serves both for further reduction of the residual voltage during RX and, more importantly, reverts the action of the first $\lambda/4$ element by extending it to a $\lambda/2$ line. Therefore, during RX, the tuning varactor 'sees' directly the probe coil. As simulations show, this mechanism is also effective off-resonance within a certain bandwidth. After tuning C_9 , C_{10} and the transmission line parameters of TL_1 in the simulation good tuning and matching can be achieved over a bandwidth of approximately 20% of f_0 . During TX an S_{11} of at least -12 dB can be achieved within this band. The reason for the larger allowable tube length is the fact that in this configuration C_9 is in parallel to C_6 . Thus the transmission line capacitance is allowed to 'consume' also part of C_9 and still provides a fair S_{11} during TX. In our practical implementation we could reach a tube length of 10 cm, which was sufficient for all our applications. As the bandwidth is considerably reduced with respect to the original implementation, we provided two different RX protecting networks with different resonance frequencies onto the same PCB and made them selectable by two jumpers. This way the band between 79 and 116 MHz can be covered with a single probehead, which corresponds to approximately 40% of the central TX frequency. One major disadvantage of this design are the additional resistive losses in the coils L_7 and L_9 which reduce the SNR by about 20% compared to the original circuit. In order to keep the losses as low as possible the coils were made from comparatively thick (0.8 mm diameter), silver-plated copper wire.

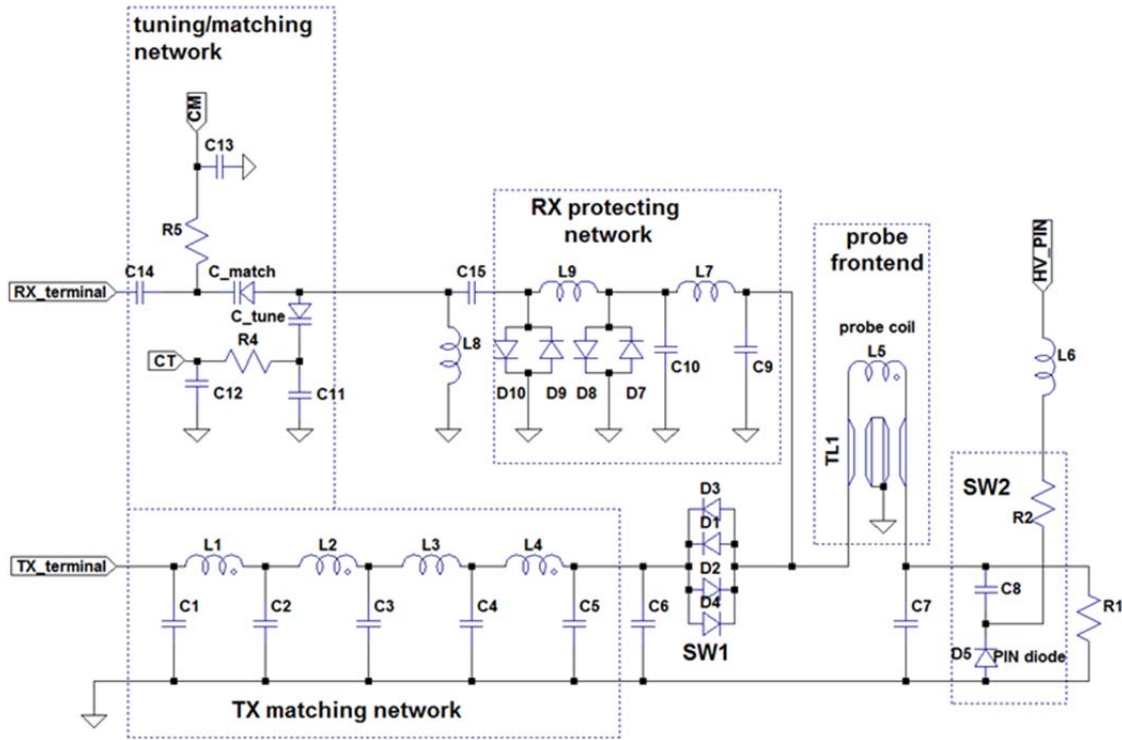


Fig. 5. Detailed schematic of the alternative circuit with passive RX protecting network.

Spectrometer

In principle the probehead can be used in combination with commercial spectrometers. In one implementation we used it with a Tecmag Scout (Tecmag, Inc., USA) using the classical technique. However, as it is difficult to program this device for the ISS, we apply this configuration only for accurate relaxometric measurements where the advanced pulse programmer of the commercial console is required. For fast explorative scans we employ the custom-made spectrometer described in [21] which relies on the network analyzer (NWA) ZWA03 (Rohde&Schwarz). For details of the data acquisition, the calibration of the tuning/matching voltages and the console program written under LABVIEW please refer to [21].

Coil characterization

The matching of the TX coil was measured by scanning the S_{11} parameter at the TX port while switching the HV_PIN control line to TX-mode and bridging SW₁ by a jumper. Measurements were done with the same NWA which was used in the spectrometer. As the useful TX bandwidth we defined the frequency range within which the return loss remained below -12dB. Moreover the Q factor was measured by measuring the S_{12} parameter between two magnetically decoupled coils (double-loop coil) which were weakly coupled to the probe coil so that a clear resonance peak could be obtained in RX mode. Q was calculated from the 3-dB bandwidth of the peak at 10 different resonance frequencies f_r within the entire RX bandwidth. The settling times of the control voltages for the varactors

and PIN diodes were checked with an oscilloscope (Tektronix TDS3014B) while measuring the rise-times at the respective points. All settling times were found to be within the requested limits.

In total we built three different probeheads according to fig. 4 and one prototype of the alternative configuration in fig. 5. Their frequency ranges and Q-factors in the middle of the respective band are summarized in table 1.

Name	Frequency range (MHz)	Q (f_{middle})	Tube length (mm)
A3	63-116	50	62
B3	34-65	51	105
C3	24-41	52	137
A4	79-116*	70	90

*Table 1: Frequency ranges and Q-factors at the central frequency f_{middle} of the respective band. *band was split into two subbands from 70 – 95 and from 95 – 116 MHz.*

Validation experiments at room temperature and in liquid nitrogen

In the framework of the research project which motivates this paper (see acknowledgement) we investigated a family of organometallic ^{209}Bi compounds which play a central role as starting materials for a potential QRE based contrast agent. From this family we chose triphenylbismuth (Sigma Aldrich) for the evaluation of our system. For comparison with our previous probeheads [21] we also measured spectra of ZnBr_2 which contains Bromine (Br) as QN with spin quantum number $I=3/2$. The solid powders were filled up to a height of 2 cm into glass cuvettes with an inner diameter of 6.5 mm and pressed gently so as to maximize the filling factor. Then the cuvettes were closed with a plastic stopper, placed inside of the coils and secured. The temperature of the samples was measured with a commercial thermoelement type K coupled to a multimeter TE.ELECTRONIC MS8264. In order to keep the temperature widely constant a continuous thermostatised airstream was passed through the PTFE tube of the probehead from top. Thermostatisation was achieved with a Peltier Temperature Controller (NMR Service GmbH, Germany). After settling to the target temperature (27.5°C for triphenylbismuth and 25°C for ZnBr_2) the ISS was used to scan over the whole accessible range between 20 and 116MHz in sub-bands with FS = 15MHz or 30 MHz and $m=150$ or 300, respectively, depending on the individual coil bandwidths. In all cases $s=10$ subspectra were acquired, corresponding to a Δf_s of 10 kHz. N was set either to 100, 200 or 500, depending on the peak amplitude within the respective sub-bands. A spin echo sequence was used with $T_E=80\text{ms}$ and $T_R'=1.5\text{ms}$. The pulse duration was chosen with $14\mu\text{s}$ for coil A3 and $8\mu\text{s}$ for coils B3 and C3 while adapting the pulse power so as to have approximate flip angles of 90°.

The experiments were repeated after plunging the respective probehead into a Dewar with LN and allowing the sample to fully equilibrate to -196.15°C (77K) for 1min. A similar

experiment was carried out for a sample of ZnBr_2 in order to show a more complex, but narrower spectrum for comparison.

3. Results

Fig. 6 shows the complete wideband spectra obtained from triphenylbismuth at 27.5 and -196.15°C in a single plot. The data from the three coils A3 – C3 were concatenated into ‘panoramic’ full datasets and plotted as raw data. The SNR of identified peaks was calculated as the ratio between the peak amplitude and the RMS value of the noise in the baseline interval. Peak amplitudes are given in μV_{RMS} received at the input of the low noise preamplifier. One can clearly distinguish the four narrow peaks labelled TR1 – TR4 which correspond to the transitions $|3/2\rangle \rightarrow |1/2\rangle$, $|5/2\rangle \rightarrow |3/2\rangle$, $|7/2\rangle \rightarrow |5/2\rangle$ and $|9/2\rangle \rightarrow |7/2\rangle$, respectively, at the frequencies 30.64; 56.44; 85.45 and 114.0 MHz at -196.15°C and 29.76, 55.21, 83.51 and 111.4 MHz, respectively, at 27.5°C. The most prominent features are the strong signal enhancement (and thus SNR gain) by a factor of up to 4 and the upward shift of the transition frequencies when decreasing the temperature from 27.5°C to -196.15°C. All transition frequencies at room temperature are in excellent agreement with those published in the Landolt-Börnstein database [32].

Though the figure enables a very accurate localization of the transition frequencies, the amplitudes of the peaks must be interpreted with caution for the following reasons:

- (1) Different coils have slightly different geometries and winding densities, therefore their filling factor and magnetic field distribution is somewhat different, leading to different sensitivity.
- (2) The magnetic flux density varies by up to 20% within the coil bandwidth and thus the flip angle is not optimal for all frequencies when scanning over very large bands such as 30 MHz. (The current spectrometer implementation does not allow for an automatic compensation of this effect).
- (3) The T_2 relaxation times vary considerably over the transitions TR1 – TR4 as well as with temperature, ranging from as short as 80 μs for TR1@27.5°C to 822 μs for TR4 @-196.15°C. Therefore the T_2 weighting is different for all peaks. The quantification and discussion of the relaxation rates, however, is beyond the scope of this paper and shall thus be left to a separate publication.
- (4) Sample positioning inside of the coil may have been subject to a certain variability.

Despite all these imperfections the relative amplitudes correspond approximately to those which can be expected from theoretical calculations of the quantum-mechanical transition probabilities, the Boltzmann populations, the transverse relaxation time constants T_2 and the induction law. The variations of the noise floor between different coils is due to the different levels of averaging (100, 200 or 500).

The total scanning time was approximately 45 min per complete spectrum, i. e. 90 min for fig. 6. The SNR varied between 51 (TR1@27.5°C) and 578 (TR3@-196.15°C).

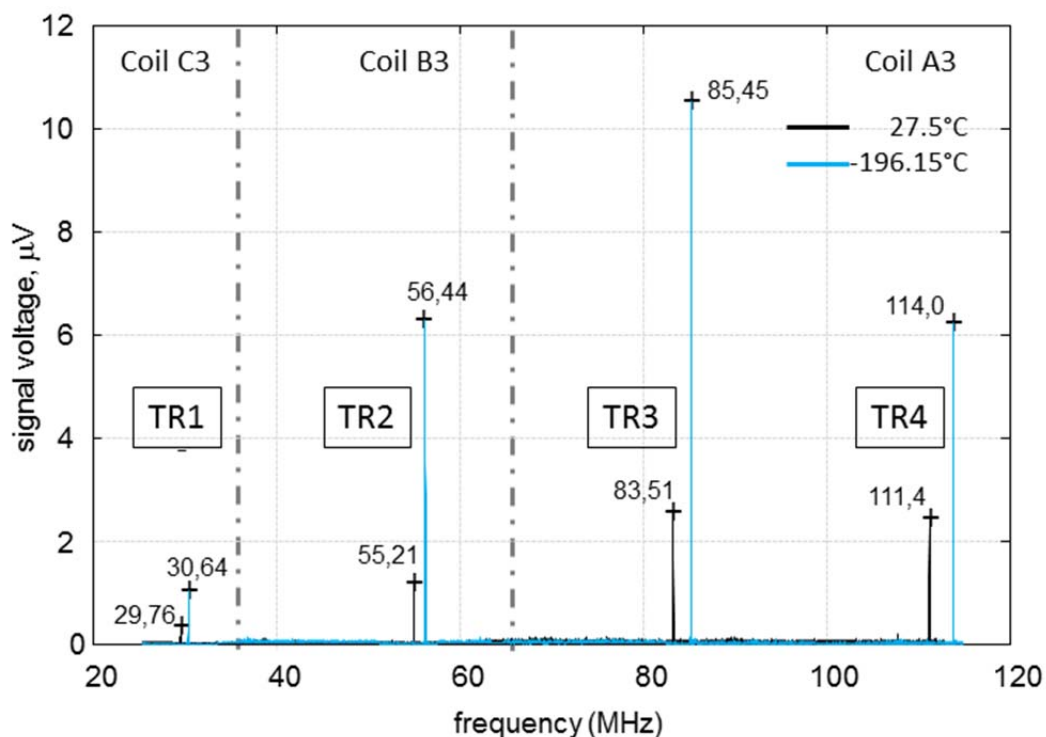


Fig. 6. Complete wideband spectra of triphenylbismuth at -196.15°C (blue) and 27.5°C (black), showing all four transitions TR1-TR4, respectively. The numbers beneath the peaks denote the respective transition frequencies in MHz. The dash-dotted vertical lines separate the bands of the three coils.

Fig. 7 shows two superimposed spectra of anhydrous ZnBr_2 at two different temperatures, i.e. 25°C and -196.15°C. As Br has a spin quantum number of 3/2 the quantum-mechanical rules allow only for one single transition. However, both spectra contain two triple peaks labelled as A1-A3, B1-B3 and A1'-A3', B1'-B3', respectively, whereby primed labels refer to the measurements at room temperature. The reason for the multiple peaks is twofold: First there exist two different Br isotopes namely ^{79}Br (label B, triple peaks above 95MHz) and ^{81}Br (label A, triple peaks below 85MHz). Second: Each triplet consists of the contributions from three different crystallographic sites in the ZnBr_2 crystallites, whereby the central peak is approximately twice as high as the two satellite peaks, see [33] for more details. The measured peak frequencies are given in table 2:

Temperature	-196.15°C			25°C		
site	1	2	3	1'	2'	3'
Isotope A	81,43	83,08	84,14	79,75	81,40	82,33
Isotope B	97,47	99,48	100,7	95,46	97,44	98,55

Table 2: Transition frequencies in MHz for the different Br isotopes and sites in $ZnBr_2$.

The data are in agreement with those published in [34].

Again the strong upshift in frequency as well as the decrease of the amplitude with decreasing temperature is clearly visible.

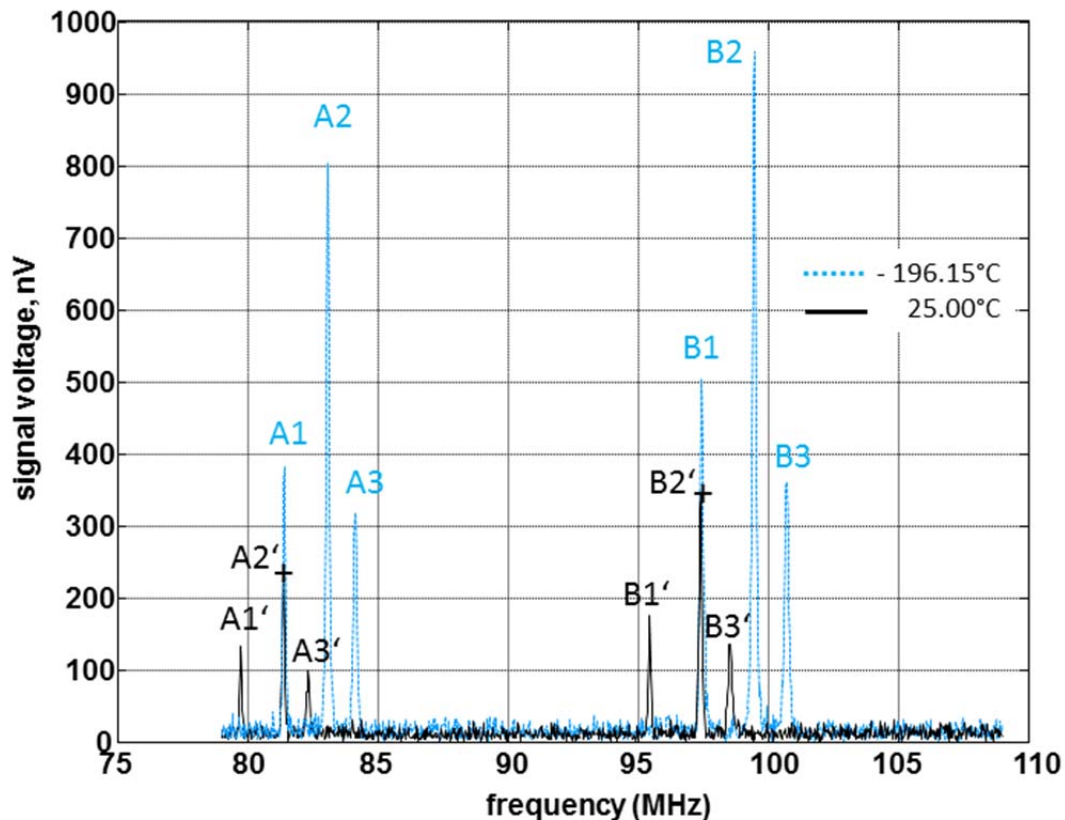


Fig. 7. Wideband spectrum of $ZnBr_2$ Anhydrid, 1000 points, 10 averages @ -196.15°C (blue/dashed) and 25 averages at 25°C (black/solid), IF BW 10kHz, span 30 MHz, classical scan, spin echo with $T_p = 22 \mu s$, $T_E = 200 \mu s$, $T_R = 3000 \mu s$.

Discussion:

We have presented a fast spectrometer for nuclear quadrupole spectroscopy in the VHF range which relies on special electronically tuneable wideband cryo-probeheads and a rapid scanning strategy (interleaved subspectrum scanning, ISS).

Complete wideband spectra of triphenylbismuth and $ZnBr_2$ have been shown. The advantage of the ISS protocol was demonstrated for the identification of transition1 in triphenylbismuth at -196.15°C, the T_1 time of which is 64ms and the signal of which is comparatively low. With the classical scan technique T_R typically would have to be set to $3 T_1$

, i. e. nearly 200 ms in order to preserve maximum SNR. With the same frequency spacing and averaging as in our experiments the scan over the band of coil C3 would require approximately 41 hours, while the ISS took only 18 min at T_R' of 1.5 ms, providing an acceleration factor of 136. Thus the classical technique may become prohibitively tedious for long T_1 at low SNR while ISS together with fast electronic tuning is very well feasible under these conditions.

There is of course also a limitation of ISS: The maximum allowable power dissipation limits s and thus the shortest allowable T_R' . In our experiments and with our coils the safe limit was given with a T_R' of around 1.5 ms. If T_1 is shorter, the ISS does not offer any significant advantage. In the case of triphenylbismuth at room temperature T_1 is only 2915 μ s for transition 1 and thus with our T_R' of 1.5 ms the acceleration factor reduces to 2-3 and at transition 4 ($T_1 = 833$ ms) there is practically no speedup any more.

The comparison so far is not completely fair because the Q-factor of a classical probehead with a simple LC-resonator can be considerably higher than the one reached with our design (typically 40-50). The main reason are the varactor diodes with their low and frequency-dependent loss factors. The Q-factor could still be increased at the cost of bandwidth, but in general the LC tank is superior, usually up to a factor of 4. Therefore, theoretically, the acceleration factor is reduced by \sqrt{Q} .

However, with the classical resonator there arises another severe limitation when it comes to samples with very short T_2 : Ringdown artefacts after TX requires a certain blanking time between the end of TX and the start of data acquisition, which prevents the detection of peaks with very fast T_2 relaxation. Fortunately, unlike in NMR, acoustic ringing [35] is not an issue because of the absence of a static magnetic field but all the other types of synchronous transient perturbations affect the data. In an ordinary resonator roughly 23 time constants τ are necessary to come down from 100 V_{pp} during TX to less than 10nV (see also [36] [37]). As derived in [38]

$$\tau = \frac{2Q_{loaded}}{\omega_0} \quad (6)$$

whereby Q_{loaded} is half the unloaded Q. Assuming an unloaded Q of 200 and a resonance frequency of 90 MHz (middle of the band of coil A3) we thus get $t = 350$ ns and a necessary blanking time of 8 μ s. In contrast, the Q-factor of our probehead is switched from approximately 2 during TX to 50 during RX thus yielding two different time constants τ_{TX} and τ_{RX} in subsequent phases. Eq. 6 then yields a τ_{TX} of ca. 7ns in coil A3 and 19.6ns for coil C3 while τ_{RX} is 75ns and 500ns, respectively. After the end of the RF pulse we implemented a short safety interval T_w of 1 μ s before switching to RX mode, thus leaving enough time (more than $50\tau_1$ for coil C3) to damp any residual oscillation below detectability when switching to RX. This mechanism can be considered as an intrinsic active ringdown quencher, thus other active quenchers suggested for high-Q tanks (see e.g. [39],[31]) were considered as

unnecessary. They could, of course, still be added in order to suppress residual leakage of low frequency ringing of the biasing network due to parasitic switching spikes, if necessary.

In our setup probeheads A and B yield reasonably small ringdown artifacts ($<50\text{nV}$) with an additional blanking time T_B of $4\mu\text{s}$ after T_W which allows for the acquisition of fast decaying FID signals. Extending T_B to $10\mu\text{s}$ eliminated the artefacts below detectability when averaging up to $N=2000$. Probehead C, as expected, requires somewhat longer blanking times. When carrying out narrowband spectroscopy with a commercial spectrometer and a commercial, motor-tuned classical probehead (Tabletop NQR Probe Autotune, NMR Service GmbH, Germany) the required blanking time was approximately the same, thus no significant difference could be found between both systems.

Further improvements could probably be achieved with more elaborated pulse techniques, or the subtraction of two immediately subsequent measurements with and without saturation of the spin population ([40], [41]). The latter technique, however, is only applicable if T_1 is significantly longer than the interpulse interval. The use of short counterphase pulses after the main RF pulse may also be considered [42], however, this method is rather complex and wideband operation may become a major challenge.

A last point is the length of the TX pulse. While with classical high-Q-resonators we can use short pulses down to $1\mu\text{s}$ for a 90° excitation at moderate powers ($100 - 500\text{W}$), the wideband probehead requires significantly longer pulses for the same flip angle because of the low Q during TX. Though this problem decreases with decreasing frequency (higher number of turns and thus higher flux density), it is intrinsic in the design and limits the detectability of peaks with short T_2 .

We shall also mention two additional, but minor caveats:

(1) Our stripline design was designed on a heuristic basis rather than using more extended simulations with specialized software. Thus there may still be room for a slight improvement of the cryo-nozzle.

(2) The NWA-based spectrometer does not allow for more elaborate pulse sequences supporting e.g. phase cycling. Therefore accurate quantitative measurements e.g. of the relaxation time constants like in [43] are not possible.

To summarize, our approach can compete in all important aspects with the classical one while it can provide significant acceleration of the total measuring time when searching for unknown NQR transitions of a newly synthesized compound. Especially for transitions with long T_1 the approach is extremely useful and the practical operation is usually less complicated than with motor-driven probeheads, which require complex control mechanisms.

Acknowledgements

This project has received funding from the European Union's *Horizon 2020 research and innovation programme* under grant agreement No 665172

References:

- [1] Z.-Y. Chen *et al.*, 'Advance of molecular imaging technology and targeted imaging agent in imaging and therapy', *BioMed Res. Int.*, vol. 2014, p. 819324, 2014.
- [2] M. M. J. Modo and J. W. M. Bulte, *Molecular and Cellular MR Imaging*. CRC Press, 2007.
- [3] G. J. Strijkers, W. J. M. Mulder, G. A. F. V. Tilborg, and K. Nicolay, 'MRI Contrast Agents: Current Status and Future Perspectives', *Anti-Cancer Agents Med. Chemistry*, vol. 7, pp. 291–305, 2007.
- [4] G.-L. Davies, I. Kramberger, and J. J. Davis, 'Environmentally responsive MRI contrast agents.', *Chem. Commun. Camb. Engl.*, vol. 49, no. 84, pp. 9704–21, 2013.
- [5] D. V. Hingorani, A. S. Bernstein, and M. D. Pagel, 'A review of responsive MRI contrast agents: 2005–2014', *Contrast Media Mol. Imaging*, vol. 10, no. 4, pp. 245–265, 2015.
- [6] P. C. M. Van Zijl and N. N. Yadav, 'Chemical exchange saturation transfer (CEST): What is in a name and what isn't?', *Magn. Reson. Med.*, vol. 65, no. 4, pp. 927–948, 2011.
- [7] E. Vinogradov, A. D. Sherry, and R. E. Lenkinski, 'CEST: From basic principles to applications, challenges and opportunities', *J. Magn. Reson.*, vol. 229, pp. 155–172, 2013.
- [8] H. V.-T. Nguyen *et al.*, 'Nitroxide-Based Macromolecular Contrast Agents with Unprecedented Transverse Relaxivity and Stability for Magnetic Resonance Imaging of Tumors', *ACS Cent. Sci.*, vol. 3, no. 7, pp. 800–811, Jul. 2017.
- [9] S. E. Ungersma *et al.*, 'Magnetic resonance imaging with T1 dispersion contrast', *Magn. Reson. Med.*, vol. 55, no. 6, pp. 1362–1371, Jun. 2006.
- [10] D. J. Lurie *et al.*, 'Fast field-cycling magnetic resonance imaging', *Comptes Rendus Phys*, vol. 11, no. 2, pp. 136–148, 2010.
- [11] P.-O. Westlund, 'The quadrupole enhanced ¹H spin-lattice relaxation of the amide proton in slow tumbling proteins', *Phys. Chem. Chem. Phys. PCCP*, vol. 12, no. 13, pp. 3136–3140, Apr. 2010.
- [12] D. Kruk, A. Kubica, W. Masierak, A. F. Privalov, M. Wojciechowski, and W. Medycki, 'Quadrupole relaxation enhancement—application to molecular crystals', *Solid State Nucl. Magn. Reson.*, vol. 40, no. 3, pp. 114–120, Oct. 2011.
- [13] O. Rabin, J. Manuel Perez, J. Grimm, G. Wojtkiewicz, and R. Weissleder, 'An X-ray computed tomography imaging agent based on long-circulating bismuth sulphide nanoparticles', *Nat. Mater.*, vol. 5, no. 2, pp. 118–122, Feb. 2006.
- [14] A. Brown, 'Bismuth Nanoparticles as Medical X-ray Contrast Agents: Synthesis, Characterization and Applications', *Diss. Theses*, Dec. 2013.
- [15] D. Freude and J. Haase, 'Quadrupole Effects in Solid-State Nuclear Magnetic Resonance', in *Special Applications*, P. D. H. Pfeifer and D. P. Barker, Eds. Springer Berlin Heidelberg, 1993, pp. 1–90.
- [16] D. Freude, 'Quadrupolar Nuclei in Solid-State Nuclear Magnetic Resonance', in *Encyclopedia of Analytical Chemistry*, John Wiley & Sons, Ltd, 2006.
- [17] J. A. Lehmann-Horn, D. G. Miljak, L. A. O'Dell, R. Yong, and T. J. Bastow, 'Rapid detection of arsenic minerals using portable broadband NQR', *Geophys. Res. Lett.*, vol. 41, no. 19, p. 2014GL061386, Oct. 2014.
- [18] R. Blinc, T. Apih, and J. Seliger, 'Nuclear quadrupole double resonance techniques for the detection of explosives and drugs', *Appl. Magn. Reson.*, vol. 25, no. 3–4, pp. 523–534, Sep. 2004.

- [19] A. Garroway *et al.*, 'Remote sensing by nuclear quadrupole resonance', *IEEE Trans. Geosci. Remote Sens.*, vol. 39, no. 6, pp. 1108–1118, Jun. 2001.
- [20] G. Kyriakidou, A. Jakobsson, K. Althoefer, and J. Barras, 'Batch-Specific Discrimination Using Nuclear Quadrupole Resonance Spectroscopy', *Anal. Chem.*, vol. 87, no. 7, pp. 3806–3811, Apr. 2015.
- [21] H. Scharfetter, 'An electronically tuned wideband probehead for NQR spectroscopy in the VHF range', *J. Magn. Reson. San Diego Calif 1997*, vol. 271, pp. 90–98, Oct. 2016.
- [22] A. P. M. Kentgens, 'Quantitative excitation of half-integer quadrupolar nuclei by a frequency-stepped adiabatic half-passage', *J. Magn. Reson.*, vol. 95, no. 3, pp. 619–625, Dec. 1991.
- [23] J. Haase and M. S. Conradi, 'Sensitivity enhancement for NMR of the central transition of quadrupolar nuclei', *Chem. Phys. Lett.*, vol. 209, no. 3, pp. 287–291, Jul. 1993.
- [24] E. van Veenendal, B. H. Meier, and A. P. M. Kentgens, 'Frequency stepped adiabatic passage excitation of half-integer quadrupolar spin systems', *Mol. Phys.*, vol. 93, no. 2, pp. 195–213, Feb. 1998.
- [25] L. A. O'Dell and R. W. Schurko, 'QCPMG using adiabatic pulses for faster acquisition of ultra-wideline NMR spectra', *Chem. Phys. Lett.*, vol. 464, no. 1–3, pp. 97–102, Oct. 2008.
- [26] R. E. Wasylshen, S. E. Ashbrook, and S. Wimperis, *NMR of Quadrupolar Nuclei in Solid Materials*. John Wiley & Sons, 2012.
- [27] T. J. Bastow and M. E. Smith, '91Zr NMR characterisation of phases in transformation toughened zirconia', *Solid State Nucl. Magn. Reson.*, vol. 1, no. 4, pp. 165–174, Nov. 1992.
- [28] M. E. Smith and J. H. Strange, 'NMR techniques in materials physics: a review', *Meas. Sci. Technol.*, vol. 7, no. 4, p. 449, 1996.
- [29] M. A. Bernstein, K. F. King, and X. J. Zhou, *Handbook of MRI Pulse Sequences*. Elsevier, 2004.
- [30] J. Mispelter, M. Lupu, and A. Briguet, *NMR Probeheads for Biophysical and Biomedical Experiments: Theoretical Principles & Practical Guidelines*. Imperial College Press, 2006.
- [31] N. S. Sullivan, P. Deschamps, P. Néel, and J. M. Vaissière, 'Efficient fast-recovery scheme for NMR pulse spectrometers', *Rev. Phys. Appliquée*, vol. 18, no. 4, pp. 253–261, Apr. 1983.
- [32] H. Chihara and N. Nakamura, '63 Bismuth', in *Nuclei Zr - Bi*, vol. 20c, K.-H. Hellwege and A. M. Hellwege, Eds. Berlin/Heidelberg: Springer-Verlag, 1989, pp. 230–243.
- [33] T. Bastow and H. Whitfield, 'Bromine nuclear quadrupole resonance in zinc bromide and in lead bromide', *Aust. J. Chem.*, vol. 27, no. 7, pp. 1397–1400, Jan. 1974.
- [34] H. Chihara and N. Nakamura, '45-151 - 45-197: Br₂HgO₆ - 2(Br₃Sb).C₁₃H₁₂', in *Nuclei Cl - Rb*, vol. 20b, K.-H. Hellwege and A. M. Hellwege, Eds. Berlin/Heidelberg: Springer-Verlag, 1988, pp. 583–592.
- [35] I. P. Gerothanassis, 'Methods of avoiding the effects of acoustic ringing in pulsed fourier transform nuclear magnetic resonance spectroscopy', *Prog. Nucl. Magn. Reson. Spectrosc.*, vol. 19, no. 3, pp. 267–329, Jan. 1987.
- [36] E. R. Andrew and K. Jurga, 'NMR probe with short recovery time', *J. Magn. Reson.* 1969, vol. 73, no. 2, pp. 268–276, Jun. 1987.

- [37] G. L. Samuelson and D. C. Ailion, 'Self-Switching Damping Circuit for Reducing Transmitter Ringdown Time in High Power Pulse NMR', *Rev. Sci. Instrum.*, vol. 41, no. 11, pp. 1601–1603, Nov. 1970.
- [38] J. B. Miller, B. H. Suits, A. N. Garroway, and M. A. Hepp, 'Interplay among recovery time, signal, and noise: Series- and parallel-tuned circuits are not always the same', *Concepts Magn. Reson.*, vol. 12, no. 3, pp. 125–136, Jan. 2000.
- [39] B. H. Suits, 'Nuclear Quadrupole Resonance Spectroscopy', in *Handbook of Applied Solid State Spectroscopy*, D. R. Vij, Ed. Springer US, 2006, pp. 65–96.
- [40] I. P. Gerothanassis, 'Simple reference baseline subtraction–90° pulse sequence for acoustic ringing elimination in pulsed fourier transform NMR spectroscopy', *Magn. Reson. Chem.*, vol. 24, no. 5, pp. 428–433, May 1986.
- [41] C. Jaeger and F. Hemmann, 'EASY: A simple tool for simultaneously removing background, deadtime and acoustic ringing in quantitative NMR spectroscopy—Part I: Basic principle and applications', *Solid State Nucl. Magn. Reson.*, vol. 57, pp. 22–28, Feb. 2014.
- [42] D. I. Hoult, 'Fast recovery, high sensitivity NMR probe and preamplifier for low frequencies', *Rev. Sci. Instrum.*, vol. 50, no. 2, p. 193, Feb. 1979.
- [43] M. Ferrari and D. Canet, '14N Pulsed nuclear quadrupole resonance. 4. Two-pulse sequences for the determination of T1 and T2 relaxation times', *Mol. Phys.*, Oct. 2009.